Progress In Electromagnetics Research C, Vol. 80, 39–54, 2018

Information Content in Inverse Source with Symmetry and Support Priors

Raffaele Solimene*, Maria A. Maisto, and Rocco Pierri

Abstract—This paper illustrates how inverse source problems are affected by certain symmetry and support priors concerning the source space. The study is developed for a prototype configuration where the field radiated by square integrable strip sources is observed in far-zone. Three symmetry priors are considered: the source is a priori known to be a real or Hermitian or even (resp. odd) function. Instead, as spatial priors we assume that the source support consists of a single or multiple disjoint domains. The role of the aforementioned priors is assessed against some *metrics* commonly used to characterise inverse source problems such as the number of degrees of freedom, the point-spread function and the "information content" measured through the Kolmogorov entropy.

1. INTRODUCTION

Inverse source problems entail dealing with the radiation operator $\mathcal{G} : s \in \mathcal{X} \to f \in \mathcal{Y}$, which links the radiating source s to the corresponding radiated field f. Actually, the problem setting requires defining not only the radiation operator $\mathcal{G}$ † but also the source and field functional spaces $\mathcal{X}$ and $\mathcal{Y}$ [1, 2]. Both these spaces depend on the domains where s and f are supported. Say $\mathcal{S}$ and Ω these supports, respectively. $\mathcal{S}$ basically represents what one a priori knows about the location of the source whereas Ω is where the radiated field is being observed. Usually, they are assumed disjoint, that is $\mathcal{S} \cap \Omega = 0$, which reflects the fact that no observations can be taken inside the source domain. $\mathcal{X}$ and $\mathcal{Y}$ can also account for some priors concerning the degree of smoothness of s and f. The case $\mathcal{X} = L_2(\mathcal{S})$ and $\mathcal{Y} = L_2(\Omega)$ is by far the more common and general adopted setting. In particular, $\mathcal{Y} = L_2(\Omega)$ is *large* enough to accommodate noise and uncertainties that can usually corrupt the radiated field observations.

Even under this general framework some priors about the source space can still be known. Hence, it is worth studying how the inverse source problem characterises when such priors are available. Here we study how certain symmetry priors affect the inverse source problem. In particular, we consider that s belongs to one of the following subspaces of $\mathcal{X}$: the set of real or the set of even (or odd) or the set of Hermitian functions. The case s which can simultaneously belong to two of such sets is addressed as well. As a further kind of priors, support information is also considered. More in detail, having fixed $m(\mathcal{S})$ (i.e., the measure of $\mathcal{S}$) we study the differences between the case $\mathcal{S}$ which is a single domain and the case $\mathcal{S} = \cup_n \mathcal{S}_n$, where $\mathcal{S}_n$ are multiple disjoint domains.

The role of the aforementioned priors is assessed against the key features of inverse source problems. In this regard, it is recalled that under the considered setting, $\mathcal{G}$ is a compact operator [3]. Compactness strongly impacts the inverse source problem from different though linked points of view. In fact, the inversion of such a class of operators is an ill-posed problem. Accordingly, the problem must be *regularized* in order to obtain *stable* reconstructions [4]. Indeed, stability is treated-off with accuracy so

Received 9 September 2017, Accepted 17 November 2017, Scheduled 2 December 2017

* Corresponding author: Raffaele Solimene (raffaele.solimene@unicampania.it).

The authors are with the Dipartimento di Ingegneria Industriale e dell'Informazione, Seconda Universit di Napoli, Aversa 81031, Italy.

† Here $\mathcal{G}$ reminds that the kernel function is provided by the relevant Green function.

that limited resolution can be achieved, whatever criterion one may want to adopt [5], even when the radiation operator is injective. Also, the data space, which coincides with the range of the radiation operator $\mathcal{R}(\mathcal{G}) \subset \mathcal{Y}$ (once the projection of the noise onto $\overline{\mathcal{R}(\mathcal{G})}^{\perp} \subset \mathcal{Y}$ has been removed) always admits a uniform finite dimensional approximation (i.e., an *n-width* $d_n(\mathcal{R}(\mathcal{G}))$ [6] which can be more or less strongly dependent on the noise level ϵ. The size of such a subspace is linked to the so-called number of degrees of freedom (NDF) [7, 8]. In short, the NDF is the number of required parameters in order to represent the radiated field with a given degree of accuracy. Changing perspective, the NDF is also related to the size of the subspace of $\mathcal{X}$ where s is stably reconstructed [9]. Hence, it affects the point-spread function and hence the achievable resolution. Compactness of the radiation operator also entails that the data space has finite packing and covering (whose sizes can be linked to the noise level ϵ) when the source space is bounded. This feature is relevant while looking at the inverse source problem under the framework of Kolmogorov topological (or metric) information theory [10]. In particular, the packing and covering of $\mathcal{R}(\mathcal{G})$ are linked to the concepts of ϵ-*capacity* and ϵ-*entropy* introduced by Kolmogorov. These basically measure the number of distinguishable fields or equivalently the number of distinguishable source functions that can be reconstructed with a given degree of accuracy.

According to previous discussion, the role of the considered priors is assessed against the NDF, the point-spread function features and the Kolmogorov entropy.

Before proceeding further, we advise the reader that, to keep math aspects as simple as possible, the study is developed under a one-dimensional setting (i.e., both s and f are functions of one variable). Also, the radiation operator is considered for the far-zone approximation. This greatly simplifies the analysis as $\mathcal{G}$ becomes a Fourier transform operator acting on functions of compact support, that is

$$f(u) = \int_{\mathcal{S}} e^{jux} s(x) dx \quad \text{with} \quad u \in \Omega = [u_{\min}, u_{\max}] \tag{1}$$

This model corresponds to the configuration depicted in Fig. 1 which refers to an electric strip current supported over $\mathcal{S}$ (assumed to be a bounded not necessarily connected domain of the x-axis) directed along the y-axis. $u = k \sin\theta$, θ is the observation angle, k the medium wavenumber, and $u_{\min}$ and $u_{\max}$ correspond to $\theta_{\min}$ and $\theta_{\max}$. $\Omega = [u_{\min}, u_{\max}]$ can be symmetric and centred (i.e., Ω_{sc} with $u_{\min} = -u_{\max}$) or mono-lateral (i.e., Ω_{ml} with $u_{\min} u_{\max} \geq 0$). The case Ω is not centred nor mono-lateral (i.e., $u_{\min} \neq -u_{\max}$ and $u_{\min} u_{\max} < 0$) which is left out the study as it can be easily derived from the two considered cases.

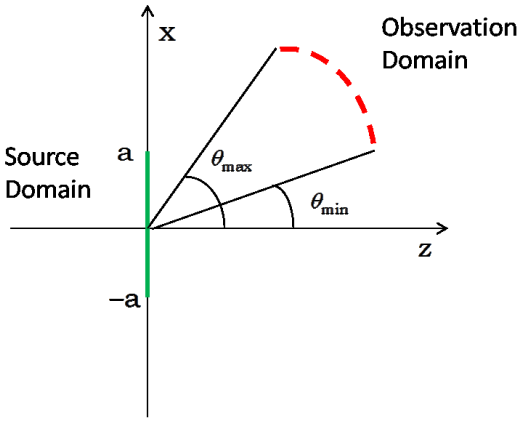

Figure 1. Geometry of the problem. The field radiated by an electric strip current directed along y and supported over the interval $\mathcal{S} = [-a, a]$ of the x-axis is collected in far zone over the observation angular sector $[\theta_{\min}, \theta_{\max}]$.

Finally, possible extensions of the presented results to different and more complex scenarios are discussed at the end of the paper.

2. PRELIMINARIES AND NOTATION

In this section some basic definitions are recalled, and the notation used throughout the paper is introduced.

$\mathcal{G}^i$ denotes a compact operator linking $\mathcal{X}$ and $\mathcal{Y}$, and $\{u_n^i, v_n^i, \sigma_n^i\}_{n=0}^{\infty}$ its singular system. The superscript i reminds the kind of prior under concern. By definition $\mathcal{G}^i u_n^i = \sigma_n^i v_n^i$ and $\mathcal{G}^{i\dagger} v_n^i = \sigma_n^i u_n^i$, $\mathcal{G}^{i\dagger}$ being the adjoint operator of $\mathcal{G}^i$, with $\overline{\mathcal{R}(\mathcal{G}^i)} \subseteq \mathcal{Y}$ and $Dom(\mathcal{G}^i) = \{s \in \mathcal{X} : \mathcal{G}^i s \neq 0\} \subseteq \mathcal{X}$ spanned by the v_n^is and u_n^is, respectively. The inversion of $\mathcal{G}^i$ can be formally expressed as

$$\tilde{s} = \sum_{n=0}^{\infty} \frac{\langle f + \mathcal{N}, v_n^i \rangle}{\sigma_n^i} u_n^i \tag{2}$$

$\mathcal{N}$ being the noise corrupting the field. As the singular values accumulate at zero, Eq. (2) needs to be regularized. This can be achieved by introducing a windowing sequences W_n which multiplies the terms within the series in Eq. (2). The simplest approach is the truncated singular value decomposition (TSVD) [4] for which $W_n = 1$ for $0 \leq n \leq N^i$ and $W_n = 0$ for $n > N^i$, N^i being the truncation index to be fixed according to "tolerable" noise level. When the singular values exhibit a step-like behaviour, N^i is *weakly* dependent on the noise and is usually addressed as the number of degree of freedom of the problem. In general, the expansion coefficients in Eq. (2) are complex. Therefore in terms of real parameters the $NDF^i = 2N^i$.

The TSVD inversion scheme leads to the following *model resolution kernel* (i.e., the point-spread function)

$$psf^i(x, x') = \sum_{n=0}^{N^i} u_n^i(x) u_n^{i*}(x') \tag{3}$$

where * means conjugation. Basically, the TSVD restricts the space where to search for the unknown current as the one spanned by the first N^i singular functions. Since now the Tikhonov topological lemma holds true the inversion procedure is stable [11].

Assume now that bounds about the norm of the noise as well as of the solution are known, that is

$$\begin{aligned} \|\mathcal{G}^i s - \tilde{f}\| &\leq \epsilon \\ \|s\| &\leq \gamma \end{aligned} \tag{4}$$

where $\tilde{f} = f + \mathcal{N}$ is the noisy radiated field. Also denote $B(0, \gamma) = \{s \in \mathcal{X} : ||s|| \leq \gamma\}$ and $\mathcal{G}^i(B(0, \gamma))$ as the image of such a hyper-sphere (which is a subset of $\mathcal{R}(\mathcal{G}^i)$) through $\mathcal{G}^i$. Let us define the ϵ-capacity, $C^i(\epsilon)$, as the maximum number of ϵ-distinguishable points (i.e., $\|g - f\| > \epsilon : g, f \in \mathcal{G}^i(B(0, \gamma))$) that belong to $\mathcal{G}^i(B(0, \gamma))$, measured in $\log_2$ scale. According to Kolmogorov, this is a measure of the (topological) information that can be transmitted from the source to the field domain [10]. Connection to the Shannon information theory was highlighted by Kolmogorov since the publication of his seminal paper and recently by the contributions of Viano and De Micheli [12].

It is clear that the $C^i(\epsilon)$ computation entails packing $\mathcal{G}^i(B(0, \gamma))$ by disjoint sets. Also, since $\mathcal{G}^i$ is compact, $C^i(\epsilon)$ is finite. A related figure which returns a lower bound for $C^i(\epsilon)$ but is easier to approximate is the ϵ-entropy $\mathcal{H}^i(\epsilon)$. In particular, $\mathcal{H}^i(\epsilon)$ is the minimum number, in $\log_2$ scale, of sets of $\mathcal{Y}$ with diameter 2ϵ which are required to cover $\mathcal{G}^i(B(0, \gamma))$. Now, if the set $\mathcal{R}(\mathcal{G}^i)$ consists of real valued functions, $\mathcal{G}^i(B(0, \gamma))$ is a hyper-ellipsoid whose axis lengths are $\sigma_n^i \gamma$, and the number of balls $B(0, \epsilon)$ required for its covering is $\prod_{n=0}^{N_\epsilon} \frac{\gamma \sigma_n^i}{\epsilon}$ with $N_\epsilon = \max\{n > 0 : \sigma_n^i \geq \epsilon/\gamma\}$ (see Fig. 2). Here, however, hyper-spheres and hyper-ellipsoids of complex valued functions are of concern. Accordingly, $\mathcal{G}^i(B(0, \gamma))$ can be regarded as the Cartesian product of two equal hyper-ellipsoids of real valued functions. Therefore, it follows that [13]

$$\mathcal{H}^i(\epsilon) \geq \log_2 \left[\prod_{n=0}^{N_\epsilon} \frac{\gamma \sigma_n^i}{\epsilon} \right]^2 = 2 \sum_{n=0}^{N_\epsilon} \log_2 \frac{\gamma \sigma_n^i}{\epsilon} \tag{5}$$

According to the previous discussion, since $\mathcal{H}^i(\epsilon) \leq C^i(\epsilon)$, Eq. (5) is used to estimate the information content. It is also possible to find an upper bound for $C^i(\epsilon)$ in terms of a majorant of $\mathcal{H}^i(\epsilon/2)$, but this is not pursued herein [13].

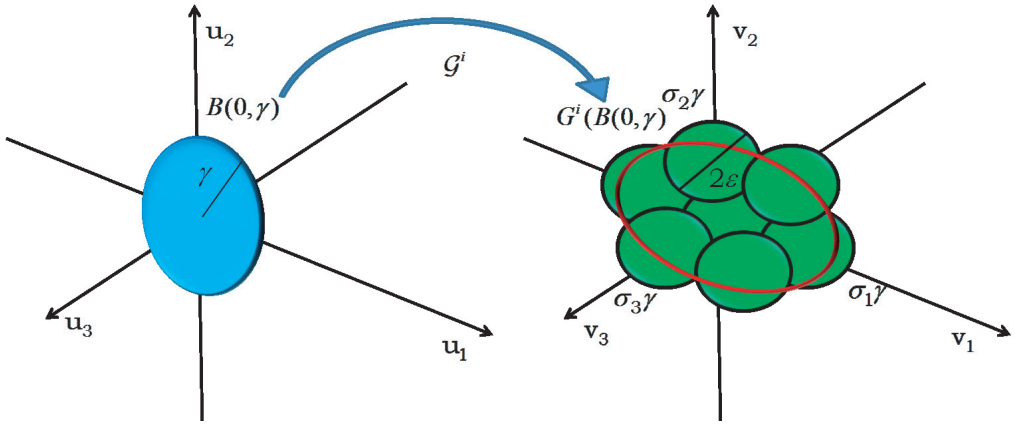

Figure 2. Graphical representation of the hyper-sphere $B(0,\gamma)$ (blue line), of its image $\mathcal{G}^i(B(0,\gamma))$ (red line) (which is a is an hyper-ellipsoid whose axis lengths are $\sigma_n^i\gamma$) through $\mathcal{G}^i$ and of balls $B(0,\epsilon)$ (green line) required for its covering. As can been seen, for the case shown in figure $N_\epsilon = 3$, this entails that to consider further dimensions does not increase the number of balls $B(0,\epsilon)$ required for the covering of hyper-ellipsoid.

It is worth noting that Eq. (5) implicitly suggests a criterion for choosing the truncation index in the TSVD expansion (3). In detail, N^i in Eq. (3) is chosen equal to N_ϵ in Eq. (5).

2.1. Benchmark Configuration

When $\mathcal{S}$ consists of a single interval, the radiation operator is denoted as $\mathcal{G}^0$. This represents the benchmark configuration against which to compare the role of priors. The singular spectrum of such an operator is well known to be linked to the prolate spheroidal wave-functions $\psi_n(\cdot,c)$ and their corresponding eigenvalues $\eta_n(c)$, $c = m(\Omega)m(\mathcal{S})/4$ being the so-called spatial-bandwidth product [14]. In particular, the singular values $\sigma_n^0 = \sqrt{2\pi\eta_n(c)}$ exhibit a step-like behaviour being nearly constant up to the index $[2c/\pi]$ [‡], beyond they decay exponentially towards zero. Therefore, for such a case, it is natural to set $N^0 = [2c/\pi]$ (hence, the number of degrees of freedom in terms of real parameters is $NDF^0 = 2(N^0+1) \simeq 2N^0$)[§], which is *weakly* dependent on the noise. This singular value behaviour entails that the inverse problem is *severely* ill-posed and reflects the properties of the kernel which is an entire function of exponential type. In fact, the more *regular* the kernel, the faster the singular values approach zero [15]. The corresponding $\mathcal{H}^0(\epsilon)$ estimation is obtained from Eq. (5) and gives [‖]

$$\mathcal{H}^0(\epsilon) \simeq 2\left(N^0+1\right)\log_2\frac{\sqrt{2\pi}}{\epsilon} \simeq 2N^0\log_2\frac{\sqrt{2\pi}}{\epsilon} \tag{6}$$

where it was considered that $\eta_n(c) \simeq 1$ for $n \leq N^0$ and, without loss of generality, and γ was assumed equal to 1. This estimation holds true for any $\epsilon < \max\sigma_n^0 = \sqrt{2\pi}$.

It is convenient for the following analysis, to rearrange $\mathcal{G}^0$ by highlighting the real and imaginary parts of f and s. Accordingly, Eq. (1) is rewritten as

$$\begin{bmatrix} f_r \\ f_{im} \end{bmatrix} = \int_{-a}^{a} \begin{bmatrix} \cos(ux) & -\sin(ux) \\ \sin(ux) & \cos(ux) \end{bmatrix} \begin{bmatrix} s_r \\ s_{im} \end{bmatrix} dx \quad u \in \Omega \tag{7}$$

This way, $\mathcal{G}^0$ can be reinterpreted as

$$\mathcal{G}^0 : \mathbf{s} = \{s_r, s_{im}\} \in L_2^{\Re}(\mathcal{S}) \times L_2^{\Re}(\mathcal{S}) \rightarrow \mathbf{f} = \{f_r, f_{im}\} \in L_2^{\Re}(\Omega) \times L_2^{\Re}(\Omega) \tag{8}$$

[‡] $[\cdot]$ denotes the operator that returns the integer part of the argument.
[§] Note that if the truncation index is N^0 the number of retained singular functions is N^0+1 as the counting index n in (3) and (5) starts from 0.
[‖] Here and throughout the text we confuse $\mathcal{H}^0(\epsilon)$ with its lower bound.

where $L_2^{\Re}$ denotes real square integrable functions. The singular spectrum of Eq. (8) can still be given in terms of the spheroidal functions (see Appendix A). However, now the singular values exhibit the step in correspondence of the index $2[2c/\pi]+1$. Accordingly, the NDF, and hence the entropy, is the same as above.

Finally, note that for the benchmark case, $\mathcal{S}$ can be considered centred with respect to $x=0$, say $\mathcal{S}=[-a,a]$. If $\mathcal{S}$ is not centred, a unitary translation operator is required which does not change the NDF^0, $\mathcal{H}^0(\epsilon)$ and the point-spread function.

3. SYMMETRY PRIORS

We start by considering symmetry priors by analysing the role of reality or evenness (resp. oddness) and Hermitianity of s on the NDF, the point-spread function and $\mathcal{H}(\epsilon)$.

3.1. Real Sources

If s is known to be a real function, the radiation operator modifies as follows, after introducing the projector P_r onto the space of real function

$$\mathcal{G}^r=\mathcal{G}^0P_r:\mathbf{s}\in L_2^{\Re}(\mathcal{S})\times L_2^{\Re}(\mathcal{S})\rightarrow\mathbf{f}\in L_2^{\Re}(\Omega)\times L_2^{\Re}(\Omega) \tag{9}$$

with

$$P_r=\begin{bmatrix}1&0\\0&0\end{bmatrix} \tag{10}$$

The explicit evaluation of $\mathcal{G}^{r\dagger}\mathcal{G}^r$ shows that (as expected) the singular functions span only s_r and are in the form $\mathbf{u}_n^r=(u_{nr}^r,0)$ with the u_{nr}^rs that verify the following integral equation

$$\sigma_n^{r2}u_{nr}^r(x)=(\mathcal{G}^{r\dagger}\mathcal{G}^ru_{nr}^r)(x)=\int_{-a}^{a}\int_{\Omega}\cos\left[u(x-x')\right]duu_{nr}^r(x')dx' \tag{11}$$

The operator in Eq. (11) can conveniently be rewritten as

$$\mathcal{G}^{r\dagger}\mathcal{G}^r=\mathcal{G}_1^r+\mathcal{G}_2^r \tag{12}$$

where

$$\mathcal{G}_1^r=2\pi\int_{-a}^{a}\cos\left(u_{avg}x\right)\frac{\sin\Delta(x-x')}{\pi(x-x')}\cos\left(u_{avg}x'\right)(\cdot)dx'\qquad x\in[-a,a] \tag{13}$$

and

$$\mathcal{G}_2^r=2\pi\int_{-a}^{a}\sin\left(u_{avg}x\right)\frac{\sin\Delta(x-x')}{\pi(x-x')}\sin\left(u_{avg}x'\right)(\cdot)dx'\qquad x\in[-a,a] \tag{14}$$

with $\Delta=m(\Omega)/2$ and $u_{avg}=(u_{\min}+u_{\max})/2$.

The eigensystem of Eq. (11) is not known in closed form except for the trivial case $u_{avg}=0$ (which corresponds to Ω_{sc}). In this case, it yields

$$\left\{\sigma_n^{r2},\mathbf{u}_n^r\right\}=\left\{2\pi\eta_m(c),\begin{bmatrix}\dfrac{\psi_n(x,c)}{\sqrt{\eta_n(c)}}\\0\end{bmatrix}\right\} \tag{15}$$

When $u_{avg}\neq 0$, the eigensystem can be approximated in terms of those associated to each single operator appearing in Eq. (12) [16]. By doing so, (see Appendix B for further details) the eigenspectrum of $\mathcal{G}^{r\dagger}\mathcal{G}^r$ can be approximated as ¶

$$\begin{aligned}\{\sigma_n^{r2},\mathbf{u}_n^r\}\approx&\left\{(1+\delta_{0,u_{avg}})\pi\eta_n(c),\begin{bmatrix}\dfrac{\sqrt{2}\psi_n(x,c)}{\sqrt{(1+\delta_{0,u_{avg}})\eta_n(c)}}\cos\left(u_{avg}x\right)]\\0\end{bmatrix}\right\}\\&\cup\left\{(1+\delta_{0,u_{avg}})\pi\eta_n(c),\begin{bmatrix}\sin\left(u_{avg}x\right)\dfrac{\sqrt{2}\psi_n(x,c)}{\sqrt{(1+\delta_{0,u_{avg}})\eta_n(c)}}\\0\end{bmatrix}\right\}\end{aligned} \tag{16}$$

¶ Eq. (16) accounts for also the case $u_{avg}=0$. In this case equality holds.

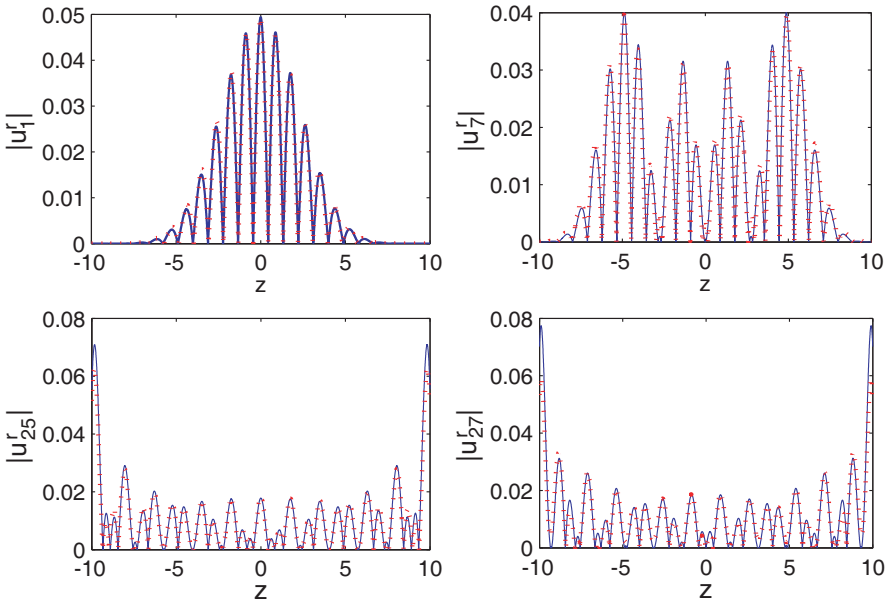

Figure 3. Comparison between the magnitude of eigenfunctions estimated by Eq. (16) (blue line) and the actual ones (red '*' lines). The parameters are $a = 10\lambda$, $u_{\min} = k\sin\pi/12$ and $u_{\max} = k\sin\pi/3$. For such a configuration $N^r = 25$. Ac can be seen the agreement is excellent not only for indexes lower than N^r (first two top panels) but also in correspondence of and beyond N^r (two bottom panels). See also discussion in Appendix B.

where $\delta_{0,u_{avg}}$ is the Kronecker delta function equal to 1 if $u_{avg} = 0$, otherwise 0. In Fig. 3, the magnitudes of some eigenfunctions estimated via Eq. (16) (blue lines) are compared to the actual (red '*' lines). As can be seen, the estimation retuned by Eq. (16) works very well and can thus be used to characterise the problem.

Equation (16) says that the singular values still exhibit a step-like behaviour with the knee occurring at $N_i^r = (2 - \delta_{0,u_{avg}})[2c/\pi] + (1 - \delta_{0,u_{avg}})$. Here, $i = (sc, ml)$. Therefore, when $u_{avg} = 0$, $NDF_{sc}^r = NDF^0/2$, whereas for $u_{avg} \neq 0$, $NDF_{ml}^r = NDF^0$. Note that since here we are dealing with sets of real functions $NDF_i^r = N_i^r + 1$. The reduction of NDF for the centred case has to be expected since the reality assumption entails that the field is an Hermitian function, and hence negative frequencies do not convey "independent" information. On the other hand, for Ω_{ml}, the NDF does not decrease, but the singular value magnitude is lowered by $\sqrt{2}$ if being compared to the benchmark case. This discussion is summarised by the examples reported in Fig. 5 (left top panel).

As to the point-spread function, using Eq. (16) in the expansion (3) yields

$$psf^r(x - x') = \frac{2}{(1 + \delta_{0,u_{avg}})} \cos u_{avg}(x - x') \frac{\sin \Delta(x - x')}{\pi(x - x')} \tag{17}$$

If $u_{avg} = 0$, the point-spread function holds the same as psf^0, though $NDF_{sc}^r = NDF^0/2$. Instead, when $u_{\min} = 0$ (for Ω_{ml}), the achievable resolution improves, even though $NDF_{ml}^r = NDF^0$. Previous results are confirmed in the right top panel of Fig. 5.

Finally, as far as the ϵ-entropy, for the case at hand, Eq. (6) returns

$$\mathcal{H}^r(\epsilon) = [2 - \delta_{0,u_{avg}})[2c/\pi] + (2 - \delta_{0,u_{avg}})] \log_2 \frac{\sqrt{2\pi}}{\sqrt{(2 - \delta_{0,u_{avg}})\epsilon}} \tag{18}$$

with $\epsilon < \sqrt{2\pi/(1 - \delta_{0,u_{avg}})}$. It is evident that the ϵ-entropy always decreases with respect to $\mathcal{H}^0(\epsilon)$. This is obvious as a priori information reduces the *uncertainty*. In particular, for Ω_{sc}, $\mathcal{H}_{sc}^r(\epsilon) = \mathcal{H}^0(\epsilon)/2$. Instead, in the mono-lateral case $\mathcal{H}_{ml}^r(\epsilon) = \mathcal{H}^0(\epsilon) - [2c/\pi] - 1$, and the entropy reduction depends on c. Entropy behaviour as ϵ varies is shown in Fig. 4.

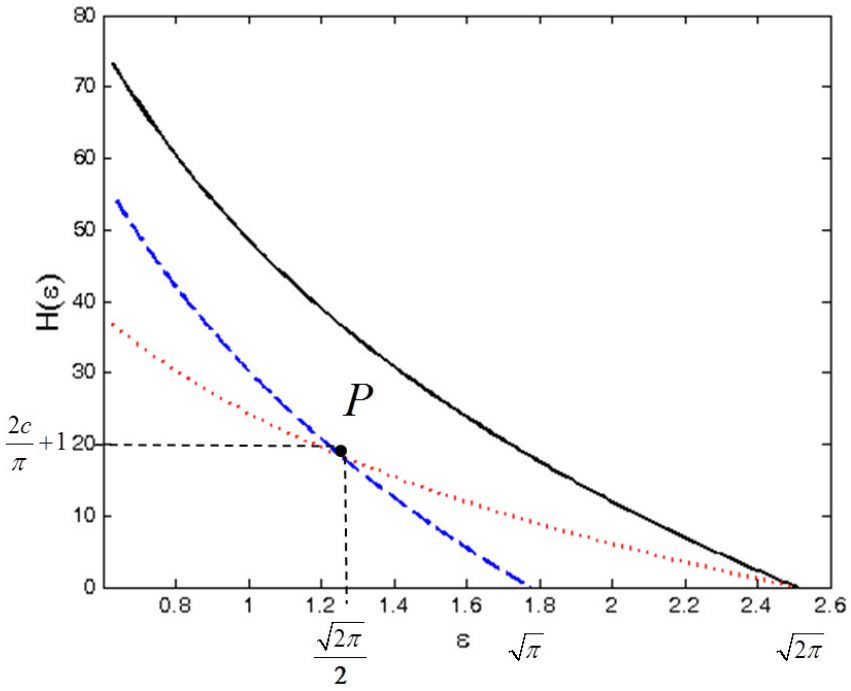

Figure 4. Comparison between $\mathcal{H}^0(\epsilon)$ (black line), $\mathcal{H}^r_{sc}(\epsilon)$ (red dot line) and $\mathcal{H}^r_{ml}(\epsilon)$ (blue dash line) as ϵ varies. The parameters are equal to the those of Fig. 5. As can be seen while $\mathcal{H}^r_{sc}(\epsilon)$ and $\mathcal{H}^r_{ml}(\epsilon)$ are always lower than $\mathcal{H}^0(\epsilon)$ with a different factor of reduction, the comparison between $\mathcal{H}^r_{sc}(\epsilon)$ and $\mathcal{H}^r_{ml}(\epsilon)$ depends by ϵ. Indeed $\mathcal{H}^r_{sc}(\epsilon)$ is greater then $\mathcal{H}^r_{ml}(\epsilon)$ when $\epsilon > \frac{\sqrt{2\pi}}{2}$, while for low values of the noise the opposite is true.

Finally, it is remarked that previous arguments hold the same for centred and not centred $\mathcal{S}$.

3.2. Hermitian Sources

The case of Hermitian s can easily be addressed starting from previous results by interchanging the role of S and Ω. In more details, now the relevant radiation operator becomes $\mathcal{G}^H = P_r\mathcal{G}^0$, so it is convenient to consider $\mathcal{G}^H\mathcal{G}^{H\dagger}$, which is formally identical to $\mathcal{G}^{r\dagger}\mathcal{G}^r$ with the role of u and x reversed. Accordingly, for Hermitian sources supported over a centred $\mathcal{S}$ one immediately obtains

$$\left\{\sigma_n^{H2}, \mathbf{v}_n^H\right\} = \left\{2\pi\eta_n(c), \begin{bmatrix} \psi_n(u-u_{avg},c)/\sqrt{\eta_n(c)} \\ 0 \end{bmatrix}\right\} \tag{19}$$

which returns $N^H_{sc} = N^H_{ml} = N^r_{sc}$ (and hence the $NDF^H = NDF^r_{sc}$) and $\mathcal{H}^H_{sc}(\epsilon) = \mathcal{H}^H_{ml}(\epsilon) = \mathcal{H}^r_{sc}(\epsilon)$.

The point spread function can be computed upon having evaluated the $\mathbf{u}_n^H$s as $1/\sigma_n^H\mathcal{G}^{H\dagger}\mathbf{v}_n^H$. Hence, by employing Eq. (3) the following point-spread function expression is found

$$\begin{aligned} psf^H(x-x') \;=\; & \frac{1}{2}\left\{\cos\left[u_{avg}(x-x')\right]\frac{\sin\Delta(x-x')}{\pi(x-x')} + \cos\left[u_{avg}(x+x')\right]\frac{\sin\Delta(x+x')}{\pi(x+x')}\right\} \\ & + \frac{j}{2}\left\{\cos\left[u_{avg}(x-x')\right]\frac{\sin\Delta(x-x')}{\pi(x-x')} - \cos\left[u_{avg}(x+x')\right]\frac{\sin\Delta(x+x')}{\pi(x+x')}\right\} \end{aligned} \tag{20}$$

As expected, the point-spread function is complex valued with the real and imaginary parts being even and odd, respectively.

If s is Hermitian and real at same time, s becomes a real even function. This situation is addressed as a particular case in the next section.

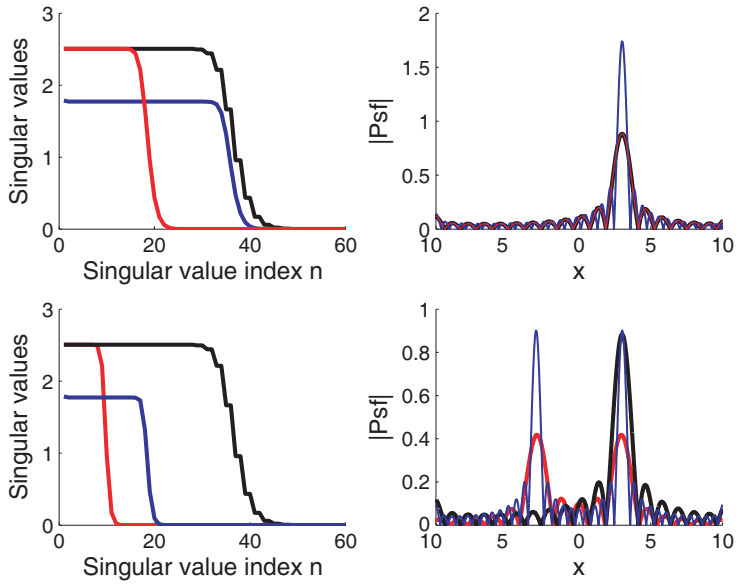

Figure 5. Illustrating the role of symmetries. The source domain is considered to be $S = [-10\lambda, 10\lambda]$, the observation domain is $\Omega_{ml} = [0, k\sin(\pi/3)]$ (blue lines) for the mono-lateral case and $\Omega_{sc} = [-\frac{k}{2}\sin(\pi/3), \frac{k}{2}\sin(\pi/3)]$ (red lines) for the symmetric centred case. In all the panels black lines refer to the benchmark case (no a priori information).
The case of a real source is considered in the top panels, where the singular values and the magnitude of the point-spread functions (pulse point located at $x' = 3\lambda$) are reported, respectively. It is seen that for Ω_{cs} the number of significant singular values is halved with respect to the benchmark, whereas for Ω_{ml} that number stays the same, but the magnitude of the singular values decreases. This is completely consistent with the theory. Also, the resolution improvement for the considered Ω_{ml} is evident.
The two bottom figures are the analogous for the case of an even source. Also here the theoretical expectations are very well verified. Note, however, that now the NDF is twice the number of the relevant singular values. Looking at the point spread function, clearly two lobes appear due to evenness. Moreover, the resolution improvement is still evident for Ω_{ml}.

3.3. Even or Odd Sources

Now the source is supposed to be even. In this case, the radiated field can be straightway written using Eq. (1) (hence, within the framework of complex valued function sets)

$$f(u) = (\mathcal{G}^e s)(u) = \int_{-a}^{a} \cos(ux) s(x) dx \quad u \in \Omega \tag{21}$$

Simple calculations show that the associated eigenvalue problem requires finding the eigenspectrum of

$$\mathcal{G}^{e\dagger}\mathcal{G}^e = \mathcal{G}_1^e + \mathcal{G}_2^e \tag{22}$$

where $\mathcal{G}_1^e$ and $\mathcal{G}_2^e$ are formally identical to $\mathcal{G}_1^r$ and $\mathcal{G}_2^r$. Accordingly, the eigenspectrum can be directly obtained from Eq. (16) by retaining only even eigenfunctions

$$\begin{aligned}\{\sigma_n^{e2}, u_n^e\} \approx &\left\{ \left(1 + \delta_{0,u_{avg}}\right) \pi \eta_{2n}(c), \frac{\sqrt{2}\psi_{2n}(x,c)}{\sqrt{(1+\delta_{0,u_{avg}})\eta_{2n}(c)}} \cos(u_{avg}x)] \right\} \\ &\cup \left\{ (1+\delta_{0,u_{avg}})\pi\eta_{2n+1}(c), \sin(u_{avg}x) \frac{\sqrt{2}\psi_{2n+1}(x,c)}{\sqrt{(1+\delta_{0,u_{avg}})\eta_{2n+1}(c)}} \right\}\end{aligned} \tag{23}$$

From Eq. (23), one deduces that for $u_{avg} = 0$ the relevant singular values are $N_{sc}^e + 1 = [N^0/2] + 1$ (the integer part operator acts only when N^0 is odd) and hence the $NDF_{sc}^e = NDF^0/2$. To be precise,

when N^0 is even, $NDF^e_{sc} = NDF^0/2 + 1$. However, we assume that $NDF^0/2 \gg 1$. Instead, for mono-lateral observation domain $N^e_{ml} = N^0$, hence $NDF^e_{ml} = NDF^0$ and the singular values magnitude is lowered by a factor $\sqrt{2}$ (see the left bottom panel of Fig. 5). Basically, the evenness prior acts on the NDF as the real one does. This can be justified by exploiting similar arguments as for the real prior with field Hermitianity replaced from parity. Also, as expected, $\mathcal{H}^e_i(\epsilon) = \mathcal{H}^r_i(\epsilon) < \mathcal{H}^0(\epsilon)$ with $i = \{sc, ml\}$. Finally, the point spread function, which of course now is even, reads as

$$psf^e(x, x') = \frac{2}{(1+\delta_{0,u_{avg}})} \times \left[\cos\left[u_{avg}(x-x')\right]\frac{\sin\left[\Delta(x-x')\right]}{\pi(x-x')} + \cos\left[u_{avg}(x+x')\right]\frac{\sin\left[\Delta(x+x')\right]}{\pi(x-x')}\right] \quad (24)$$

As in the previous section when $u_{min} = 0$ (for Ω_{ml}), the main beam results are halved as compared to the one of psf^0. However now, at variance of the reality prior, when $x' \leq \pi/\Delta$ the peaks do not occur at the right positions because the main lobes of the two terms in Eq. (24) interfere. These results are confirmed by the examples reported in the bottom panels of Fig. 5.

When the source is odd, previous results still hold but for a minus sign between the two terms of the point spread function, which accounts for the oddness of the reconstruction.

Finally, s can be simultaneously real and even (resp. odd). Merging previous results and those in Section (3.1), the radiation operator can be expressed as

$$\mathcal{G}^{re} = \mathcal{G}^e P_r : \mathbf{s} \in L^{\Re}_2(\mathcal{S}) \times L^{\Re}_2(\mathcal{S}) \rightarrow \mathbf{f} \in L^{\Re}_2(\Omega) \times L^{\Re}_2(\Omega) \quad (25)$$

It immediately follows that

$$\left\{\sigma^{re2}_n, \mathbf{u}^r_n\right\} \approx \left\{\sigma^{e2}_n, \begin{bmatrix} u^e_n(x) \\ 0 \end{bmatrix}\right\} \quad (26)$$

and hence $NDF^{re}_i = NDF^r_i/2 = NDF^e_i/2$ and $\mathcal{H}^{re}_i(\epsilon) = \mathcal{H}^r_i(\epsilon)/2 = \mathcal{H}^e_i(\epsilon)/2$ with $i = \{sc, ml\}$.

3.4. Summarising Discussion

At this juncture it is useful to collect the results obtained so far (see Table 1).

First, as expected the different considered priors lead to a reduction of the information content. Indeed, we have shown that $\mathcal{H}^r_i(\epsilon) = \mathcal{H}^e_i(\epsilon) < \mathcal{H}^0(\epsilon)$. In particular, analytical estimations quantified such a reduction. As to the NDF, once again the reality and evenness (or oddness) constraints play a similar role. In fact, $NDF^r_i = NDF^e_i$. Moreover, they are equal to NDF^0 for Ω_{ml} and reduced to $NDF^0/2$ for centred symmetric observation domain. The Hermitian prior behaves similarly for Ω_{sc} and Ω_{ml}. When real and evenness priors are both considered $NDF^{re}_i = NDF^r_i/2 = NDF^e_i/2$ and $\mathcal{H}^{re}_i(\epsilon) = \mathcal{H}^r_i(\epsilon)/2 = \mathcal{H}^e_i(\epsilon)/2$. As far as the point spread function is concerned, it has been shown that in the case of the NDF lower than NDF^0, it (and hence resolution) remains unchanged. Meaning that the lost of NDF is compensated someway by the available priors. What is more, for mono-lateral Ω_{ml} and in particular for $u_{\min} = 0$ resolution is even better than for psf^0. This is interesting as it shows that the common belief that the more the information content the better the resolution actually does not hold true.

4. SUPPORT PRIORS

In this section, we turn to consider priors about $\mathcal{S}$. If this consists of a single interval, a priori information concerns $m(\mathcal{S})$. This situation can be easily addressed in terms of well-known features of prolate spheroidal functions. Indeed, having fixed Ω, as long as c is sufficiently greater than one, then both the NDF and entropy vary linearly with $m(\mathcal{S})$, whereas the point-spread function depends solely on Ω.

Here, we are interested in studying the case $\mathcal{S} = \cup_l \mathcal{S}_l$ with $\mathcal{S}_l \cap \mathcal{S}_{l'} = 0$. For such a case, the radiation operator is denoted as $\mathcal{G}^s$ and of course is formally identical to Eq. (1) but with the integration extended over multiple disjoint intervals of the x-axis.

It is noted that the problem at hand is strictly connected to the study of multiband signals [17] and in particular to the closeness of sequences of exponential characters over compact domains [18]. In this framework, sampling and interpolating sets of points are of concern. We do not dwell on these aspects though they are of great theoretical and practical importance. What matters here is that the study

Table 1. The NDF, the point-spread function and $\mathcal{H}(\epsilon)$ when the analysed symmetry priors about the sources are considered.

	NDF	$\mathcal{H}(\epsilon)$	Point-spread function
Benchmark	NDF^0	$\mathcal{H}(\epsilon)^0$	$e^{-ju_{avg}(x-x')}\frac{\sin\Delta(x-x')}{\pi(x-x')}$
Real sources			
$\Omega=\Omega_{sc}$	$NDF^0/2$	$\mathcal{H}(\epsilon)^0/2$	$\frac{\sin\Delta(x-x')}{\pi(x-x')}$
$\Omega=\Omega_{ml}$	NDF^0	$\mathcal{H}^0(\epsilon)-[2c/\pi]-1$	$2\cos u_{avg}(x-x')\frac{\sin\Delta(x-x')}{\pi(x-x')}$
Hermitian sources	$NDF^0/2$	$\mathcal{H}(\epsilon)^0/2$	$\frac{(1+j)}{2}\cos\left[u_{avg}(x-x')\right]\frac{\sin\Delta(x-x')}{\pi(x-x')}$ $+\frac{(1-j)}{2}\cos\left[u_{avg}(x+x')\right]\frac{\sin\Delta(x+x')}{\pi(x+x')}$
Even sources			
$\Omega=\Omega_{sc}$	$NDF^0/2$	$\mathcal{H}(\epsilon)^0/2$	$\frac{\sin\Delta(x-x')}{\pi(x-x')}+\frac{\sin\Delta(x+x')}{\pi(x+x')}$
$\Omega=\Omega_{ml}$	NDF^0	$\mathcal{H}^0(\epsilon)-[2c/\pi]-1$	$2\cos\left[u_{avg}(x-x')\right]\frac{\sin\Delta(x-x')}{\pi(x-x')}$ $+2\cos\left[u_{avg}(x+x')\right]\frac{\sin\Delta(x+x')}{\pi(x+x')}$
Even and real sources			
$\Omega=\Omega_{sc}$	$NDF^0/4$	$\mathcal{H}(\epsilon)^0/4$	$\frac{\sin\Delta(x-x')}{\pi(x-x')}+\frac{\sin\Delta(x+x')}{\pi(x+x')}$
$\Omega=\Omega_{ml}$	$NDF^0/2$	$\frac{\mathcal{H}^0(\epsilon)-[2c/\pi]-1}{2}$	$2\cos\left[u_{avg}(x-x')\right]\frac{\sin\Delta(x-x')}{\pi(x-x')}$ $+2\cos\left[u_{avg}(x+x')\right]\frac{\sin\Delta(x+x')}{\pi(x+x')}$

of the density of the sampling and interpolating sets gives us useful tools to solve our problem easily. In this regard, it suffices to mention the work of Landau [19] who linked the density problem to the eigenvalue behaviour of certain operator, which in turn, incidentally, is relevant for the problem at hand. Therefore, according to Landau, N^s and $\mathcal{H}^s(\epsilon)$ are practically identical to those corresponding to $\mathcal{G}^0$, however, with $m(\mathcal{S})=\sum_l m(\mathcal{S}_l)$. Hence, it can be concluded that, having fixed $m(\mathcal{S})$, single or multiple disjoint source domains are equivalent as far as the NDF and information content are concerned.

The same result can be arrived at by exploiting the tools developed in [20], which allows to also get an estimation for the singular functions. In detail, say $\mathcal{S}$ consists of L disjoint domains. The relevant radiation operator is

$$\mathcal{G}^s=\int_{\cup_{l=1}^{L}\mathcal{S}_l} e^{jux}s(x)dx \quad \text{with} \quad u\in\Omega=[u_{\min},u_{\max}] \tag{27}$$

It is convenient to look at the problem in the field space. Hence, consider the operator $\mathcal{G}^s\mathcal{G}^{s\dagger}$ which writes as

$$\mathcal{G}^s\mathcal{G}^{s\dagger}=\sum_{l=1}^{L}2\pi\int_{\Omega}e^{jx_{avgl}(u-u')}\frac{\sin\Delta_{xl}(u-u')}{\pi(u-u')}du'=\sum_{l=1}^{L}\mathcal{G}_l^0\mathcal{G}_l^{0\dagger} \quad u\in\Omega \tag{28}$$

where $\mathcal{S}_l=[x_{avgl}-\Delta_{xl},x_{avgl}+\Delta_{xl}]$, $\Delta_{xl}=m(\mathcal{S}_l)/2$ and $\mathcal{G}_l^0$ refers to the radiation operator when the source is supported only over $\mathcal{S}_l$. The eigenspectrum of Eq. (28) has been studied in a number of recent papers (see for example [16] and [21]). It has been shown that, if the spatial-bandwidth product $c_l^s=m(\Omega)\Delta_{xl}/2$ associated with each domain is sufficiently greater than one (indeed $c_l^s>4$ is enough [16]), then

$$\mathcal{G}_l^0\mathcal{G}_l^{0\dagger}v_{nl'}^0\approx 0 \quad \forall l,l'\in\{1,\dots,L\} \tag{29}$$

with $v_{nl}^0=\frac{\sqrt{2}\psi_n(u-u_{avg},c_l^s)}{\sqrt{\eta_n(c_{l'}^s)}}e^{j[x_{avgl}(u-u_{avg})]}$ being the eigenfunctions of $\mathcal{G}_l^0\mathcal{G}_l^{0\dagger}$. Accordingly, the eigenspectrum of $\mathcal{G}^s\mathcal{G}^{s\dagger}$ is very well approximated by the union of the eigenspectra of each single $\mathcal{G}_l^0\mathcal{G}_l^{0\dagger}$.

Hence, it results in that

$$\{\sigma_n^{s2}, v_n^s\} \approx \bigcup_{l=1}^{L} \{\sigma_{hl}^{02}, v_{hl}^0\} \tag{30}$$

where n indexes the "overall" sequence $\bigcup_{l=1}^{L}\{\sigma_{hl}^{02}\}$ once ordered in non-increasing way. The eigenvalues of each $\mathcal{G}_l^0\mathcal{G}_l^{0\dagger}$ clearly exhibit a step behaviour. In particular, the singular values preceding the knee are $N_l^0 + 1 = [2c_l^s/\pi] + 1$. Therefore, it can be concluded that the "overall" number of relevant singular values is $\sum_{l=1}^{L}[2c_l^s/\pi] + L$. On the other hand, $N^0 + 1 = [2\sum_{l=1}^{L} c_l^s/\pi] + 1$. Therefore, upon noting that $2\sum_{l=1}^{L} c_l^s/\pi < \sum_{l=1}^{L}[2c_l^s/\pi] + L$, one finds that

$$\left[2\sum_{l=1}^{L} c_l^s/\pi\right] + 1 - \sum_{l=1}^{L}[2c_l^s/\pi] - L < \left[2\sum_{l=1}^{L} c_l^2/\pi\right] + 1 - 2\sum_{l=1}^{L} c_l^s/\pi < 2 \tag{31}$$

Therefore, the number of relevant singular functions differs at most by one. Accordingly, it can be concluded that $NDF^s \simeq NDF^0$ and $\mathcal{H}(\epsilon)^s \simeq \mathcal{H}(\epsilon)^0$. In order to estimate the point-spread function, the singular functions that span the unknown source must be determined through $1/\sigma_n^s \mathcal{G}^{s\dagger} v_n^s$. Simple calculations show that

$$psf^s(x, x') \approx \exp\left[-ju_{avg}(x - x')\right] \frac{\sin\left[\Delta(x - x')\right]}{\pi(x - x')} \tag{32}$$

which, according to previous discussion, is identical to psf^0.

We have shown that having fixed the measure of the source domain and under the assumptions mentioned above, a single "long" source or multiple disjoint sources are essentially equivalent. It can be easily (but tediously) shown that this holds the same when symmetry constraints are added to support priors. We show this by a numerical example. Fig. 6 illustrates previous discussion according to the same rationale used in Fig. 5. However, now the source domain consists of two disjoint intervals $\mathcal{S}_1 = [\lambda, 6\lambda]$ and $\mathcal{S}_2 = [-6\lambda, -\lambda)]$. As can be seen, by comparing Fig. 5 and Fig. 6, singular values are only slightly different beyond the knees (this, however, is consistent with our arguments in Eq. 29). Also the main lobes of the corresponding psfs are practically the same as Fig. 5.

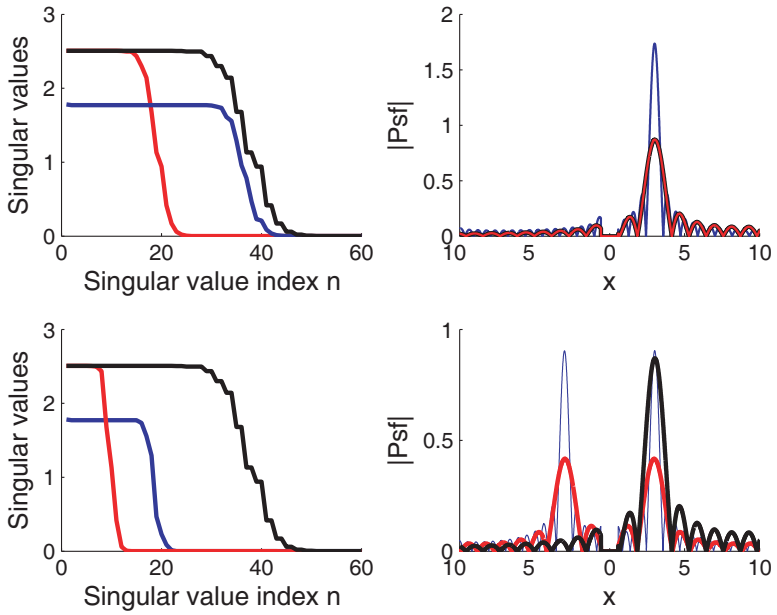

Figure 6. Here it is reported the same comparison as Fig. 5. However, now the source is supported over two disjoint intervals $\mathcal{S}_1 = [\lambda, 6\lambda]$ and $\mathcal{S}_2 = [-6\lambda, -\lambda)]$.

5. POSSIBLE EXTENSIONS

A natural question that arises is the possibility of generalising the presented study to other possibly more complex configurations, such as the case in which the observation domain is no more located in far zone or the case that the source is supported over a 2D domain, or for linear inverse scattering problems. Another interesting case could be when the source is located close to a reflecting mirror.

In this regard, while the presented results are actually specific to the particular considered configuration the developed tools are not. This is because results concerning the prolate spheroidal spectrum can again be exploited fruitfully. This is immediate, for example, in the case that the source is above a reflecting mirror [21] or for scattering problems under the Born approximation [22].

Actually, also for the near zone configuration the study can be easily generalised. Indeed, for near zone configuration, the radiation operator is more complex than a simple Fourier transform, and actually its singular spectrum cannot be derived in closed form. Nonetheless, in [23] we succeeded in finding a couple of operators whose spectra upper and lower bound one of the radiation operator. In particular, we have shown that those spectra can still be given in terms of the prolate spheroidal wave-functions. Therefore, the role of priors can be assessed by the following similar arguments (as above) but reasoning on these "bounding" operators.

A similar technique can be exploited while considering a 2D source. To make this clearer, we dwell on a few details.

Consider the 2D source and the radiation configuration depicted in Fig. 7. Assume that the source is supported over the subset $\mathcal{S} = [-a, a] \times [-b, b]$ of $\Re^2$ within the x-y plane. Also, the source is in general a vector in the same plane, i.e., $\underline{s}(x, y) = [s_x(x, y), s_y(x, y)]$ [+]. The radiated field (tangent components) $\underline{f}(x, y) = [f_x(x, y), f_y(x, y)]$ is collected over a measurement aperture Σ located at z_o. Introducing spherical coordinates, the radiation operator can be expressed as

$$\underline{f}(\theta, \phi) = -j\frac{k\zeta e^{-jkr(\theta,\phi)}}{2\pi r(\theta, \phi)}\underline{\underline{T}}(\theta, \phi)\int_{\mathcal{S}} e^{jk\sin\theta(x\cos\phi+y\sin\phi)}\underline{f}(x, y)dxdy \tag{33}$$

with

$$\underline{\underline{T}}(\theta, \phi) = \begin{bmatrix} \cos^2\theta\cos^2\phi + \sin^2\phi & -\sin^2\theta\sin\phi\cos\phi \\ -\sin^2\theta\sin\phi\cos\phi & \cos^2\theta\cos^2\phi + \cos^2\phi \end{bmatrix}$$

and ζ is the medium impedance. If $\theta \neq \pi/2$, the matrix $\underline{\underline{T}}(\theta, \phi)$ is not singular, and Eq. (33) can be rearranged as

$$\underline{\hat{f}}(\theta, \phi) = \zeta k^2 \int_{\mathcal{S}} e^{jk\sin\theta(x\cos\phi+y\sin\phi)}\underline{s}(x, y)dxdy \tag{34}$$

where $\underline{\hat{f}} = j2\pi kre^{jkr}\underline{\underline{T}}^{-1}\underline{f}$. At this juncture, the problem has been greatly simplified as the vectorial

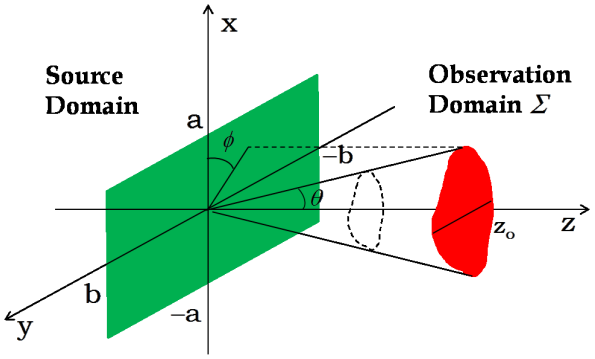

Figure 7. Schematic view of the 2D configuration. The observation domain is still considered in far zone.

[+] Note that here vectors are denoted through underline signs.

operator in Eq. (33) is transformed in two decoupled and identical scalar problems of the type

$$\hat{f}_p(u,v) = (\mathcal{G}^{2D} s_p)(u,v) = \zeta k^2 \int_{\mathcal{S}} e^{[j(ux+vy)]} s_p(x,y) dxdy \quad \text{with } (u,v) \in \Omega \text{ and } p \in \{x,y\} \tag{35}$$

with $u = k\sin\theta\cos\phi$ and $v = k\sin\theta\sin\phi$ and Ω which depends on Σ. It is seen that now Eq. (35) is cast as a couple of 2D Fourier transforms supported over a compact domain. If Σ is a rectangular aperture and Ω also rectangular and since the spectrum of $\mathcal{G}^{2D}$ can be given as the product of the prolate spheroidal spectrum, one can easily generalise the results presented herein. When the measurement aperture is not rectangular, the prolate spectrum theory cannot be applied straightway. This problem can be easily circumvented if one contents to find upper and lower bounds for the spectrum at hand. In details, define $\hat{\Omega}$ and $\tilde{\Omega}$ as two rectangular domains such that $\hat{\Omega} \supset \Omega \supset \tilde{\Omega}$. Let $\hat{\mathcal{G}}^{2D}$ and $\tilde{\mathcal{G}}^{2D}$ be the operators given by Eq. (35) when $\hat{\Omega}$ and $\tilde{\Omega}$ are considered as observation domains. Then, it can be shown that $\sigma_n(\tilde{\mathcal{G}}^{2D}) \leq \sigma_n(\mathcal{G}^{2D}) \leq \sigma_n(\hat{\mathcal{G}}^{2D})$. The point is that the spectra of $\hat{\mathcal{G}}^{2D}$ and $\tilde{\mathcal{G}}^{2D}$ can be once again given in terms of prolate functions. Therefore, one can easily generalise results presented herein by working on the "bounding" operators.

6. CONCLUSIONS

This paper has illustrated how certain symmetry and support priors affect the NDF, the point-spread function and the Kolmogorov entropy with respect to the case of no a priori information. To this end, a prototype configuration has been considered.

As expected, priors reduce the entropy and hence the information content. Here, we have given a measure of such decrease, showing that more severe reduction is obtained for symmetric centred Ω.

As to the NDF, the reality and evenness (or oddness) constraints affect, in similar manner, this parameter. In particular, a very important role is played by the observation domain. Indeed, when Ω is centred ($u_{avg} = 0$), the reality and/or evenness (or oddness) of the source entail that the NDF decreases while the point-spread function does not change, meaning that the lost of NDF is compensated someway by the available priors. Moreover, this occurs also when the source is Hermitian, regardless whether Ω is centred or not. For $u_{avg} \neq 0$, the NDF does not change as compared to the case of no prior information when the source is supposed to be even or real. Instead, it continues to decrease if s is simultaneously real and even. As to the point-spread function, its main lobe is halved, but at the same time an increase of the side-lobe level is obtained. This effect can be eliminated if the observation angular sector encompasses $\theta = 0$. This is interesting as it shows that a common belief under which the more the information content, the better the resolution actually does not hold true. Note that, in both cases, when the source is even or odd for pulse location at $x' \leq \pi/\Delta$, the peaks of the point-spread function do not occur at the right positions.

Finally, it is shown that previous results hold almost the same even when $\mathcal{S}$ consists of multiple disjoint domains of length $\sum_n m(\mathcal{S}_n) = m(\mathcal{S})$. This actually is true as long as the spatial-bandwidth product corresponding to each $\mathcal{S}_n$ is > 1.

As mentioned above, though the derived results are specific to the simple considered prototype configuration, the techniques can be applied to generalise them to more complex radiation or scattering scenarios. In this regard, some cases of potential interest have been briefly sketched above. However, we left the in-depth study of such cases in possible future works.

APPENDIX A.

In this appendix the singular spectrum of the operator $\mathcal{G}^0$ reported in Eq. (8) is derived. To this end, the eigenspectrum of $\mathcal{G}^{0\dagger}\mathcal{G}^0$ is considered by addressing the following equation

$$\mathcal{G}^{0\dagger}\mathcal{G}^0 \mathbf{u}_n^0 = \sigma_n^{02} \mathbf{u}_n^0 \tag{A1}$$

Simple manipulations allow to explicitly write Eq. (A1) as

$$2\pi \int_{-a}^{a} \begin{bmatrix} \dfrac{\sin\Delta(x-x')}{\pi(x-x')} & 0 \\ 0 & \dfrac{\sin\Delta(x-x')}{\pi(x-x')} \end{bmatrix} \tilde{\mathbf{u}}_n^0(x') = \sigma_n^{02} \tilde{\mathbf{u}}_n^0(x) \tag{A2}$$

where $\Delta = (u_{\max} - u_{\min})/2$, $u_{avg} = (u_{\max} + u_{\min})/2$ and $\begin{bmatrix} \cos(u_{avg}x) & \sin(u_{avg}x) \\ -\sin(u_{avg}x) & \cos(u_{avg}x) \end{bmatrix} \tilde{\mathbf{u}}_n^0(x) = \mathbf{u}_n^0(x)$. Finally,

$$\begin{aligned} \tilde{\mathbf{u}}_n^0 &= \begin{bmatrix} \psi_n(x,c)/\sqrt{\eta_n(c)} \\ 0 \end{bmatrix} \cup \begin{bmatrix} 0 \\ \psi_n(x,c)/\sqrt{\eta_n(c)} \end{bmatrix} \\ \sigma_n^{02} &= 2\pi\eta_n(c) \end{aligned} \tag{A3}$$

with each σ_n^{02} having multiplicity 2 and $\mathbf{v}_n^0(u) = [(\mathcal{G}_0\mathbf{u}_n^0)(u)]/\sigma_n^0$.

APPENDIX B.

In order to approximate the eigenspectrum of Eq. (12) for the case $u_{avg} \neq 0$, we start by approximating those of $\mathcal{G}_1^r$ and $\mathcal{G}_2^r$. Both these operators are compact, symmetric and positive definite. Hence, by Mercer theorem, their kernel functions G^1 and G^2 admit uniform convergent expansions in terms of their eigenfunctions [24]. For the same reason, $\sin[\Delta(x-x')]/\pi(x-x')$ can be expanded through prolate functions. Accordingly,

$$G^1(x,x') = \sum_n \pi\eta_n(c)\cos(u_{avg}x)\frac{\sqrt{2}\psi_n(x,c)}{\sqrt{\eta_n(c)}}\cos(u_{avg}x')\frac{\sqrt{2}\psi_n(x',c)}{\sqrt{\eta_n(c)}} \tag{B1}$$

and

$$G^2(x,x') = \sum_n \pi\eta_n(c)\sin(u_{avg}x)\frac{\sqrt{2}\psi_n(x,c)}{\sqrt{\eta_n(c)}}\sin(u_{avg}x')\frac{\sqrt{2}\psi_n(x',c)}{\sqrt{\eta_n(c)}} \tag{B2}$$

Unfortunately, Eqs. (B1) and (B2) are not Mercer expansions as the involved functions are not all orthogonal. More precisely,

$$\left\langle \cos(u_{avg}x)\frac{\sqrt{2}\psi_n(x,c)}{\sqrt{\eta_n(c)}}, \cos(u_{avg}x)\frac{\sqrt{2}\psi_m(x,c)}{\sqrt{\eta_m(c)}} \right\rangle = \delta_{n,m} + \frac{\left[\hat{\psi}_m \star \hat{\psi}_n(2u_{avg}) - \hat{\psi}_m \star \hat{\psi}_n(-2u_{avg})\right]}{\sqrt{\eta_n(c)\eta_m(c)}} \tag{B3}$$

$$\left\langle \sin(u_{avg}x)\frac{\sqrt{2}\psi_n(x,c)}{\sqrt{\eta_n(c)}}, \sin(u_{avg}x)\frac{\sqrt{2}\psi_m(x,c)}{\sqrt{\eta_m(c)}} \right\rangle = \delta_{n,m} - \frac{\left[\hat{\psi}_m \star \hat{\psi}_n(2u_{avg}) - \hat{\psi}_m \star \hat{\psi}_n(-2u_{avg})\right]}{\sqrt{\eta_n(c)\eta_m(c)}} \tag{B4}$$

where $\hat{\psi}_n$ denotes the Fourier transform of ψ_n when this is supported over $[-a,a]$, and $\star$ means convolution. For $n,m \leq [2c/\pi]$, the second terms in the right hand side of Eqs. (B3) and (B4) are zero because $\hat{\psi}_m \star \hat{\psi}_n$ is just supported over $[-2\Delta, 2\Delta]$ and $2\Delta \leq 2u_{avg}$. Therefore, $\{\pi\eta_n(c), \sqrt{2}\cos(u_{avg}x)\psi(x,c)/\sqrt{\eta_n(c)}\}_{n=0}^{[2c/\pi]}$ and $\{\pi\eta_n(c), \sqrt{2}\sin(u_{avg}x)\psi(x,c)\sqrt{\eta_n(c)}\}_{n=0}^{[2c/\pi]}$ actually belong to the eigenspectra of $\mathcal{G}_1^r$ and $\mathcal{G}_2^r$, respectively. What is more, such finite dimensional portions of the spectra capture all the nuclear norm (i.e., the trace) of such operators. In view of the positivity of such operators, this entails that for $n > [2c/\pi]$ the eigenvalues must decay abruptly towards zero (step-like behaviour). Hence, the corresponding spectrum is of minor importance. Accordingly, the eigenspectra at hand can be approximated as

$$\left\{ \pi\eta_n(c), \frac{\sqrt{2}\psi_n(x,c)}{\sqrt{\eta_n(c)}}\cos(u_{avg}x) \right\} \tag{B5}$$

for $\mathcal{G}_1^r$ and as

$$\left\{ \pi\eta_n(c), \frac{\sqrt{2}\psi_n(x,c)}{\sqrt{\eta_n(c)}}\sin(u_{avg}x) \right\} \tag{B6}$$

for $\mathcal{G}_2^r$.

Finally, it is noted that for $n \leq [2c/\pi]$

$$\| \mathcal{G}_1^r \psi_n(x,c)\sin(u_{avg}x) \| = 0 \tag{B7}$$

and

$$\| \mathcal{G}_2^r \psi_n(x,c) \cos(u_{avg}x) \| = 0 \tag{B8}$$

This can be easily shown by using the same arguments as in Eqs. (B3) and (B4). Note that Eqs. (B7) and (B8) also entail that

$$\langle \psi_n(x,c) \cos(u_{avg}x), \psi_n(x,c) \sin(u_{avg}x) \rangle = 0 \tag{B9}$$

For $n > [2c/\pi]$, Eqs. (B7) and (B8) are ≈ 0 because $||\psi_n|| \approx 0$ when the prolate functions are restricted to $[-a, a]$. Hence, the eigenspectrum approximation in Eq. (16) arises.

REFERENCES

1. Soldovieri, F., C. Mola, R. Solimene, and R. Pierri, "Inverse source problem from the knowledge of radiated field over multiple rectilinear domains," *Progress In Electromagnetics Research M*, Vol. 8, 131–141, 2009.
2. Solimene, R., C. Mola, R. Pierri, and F. Soldovieri, "Inverse source problem: A comparison between the cases of electric and magnetic sources," *Progress In Electromagnetics Research M*, Vol. 20, 127–141, 2011.
3. Kantorovic, L. V. and G. P. Akilov, *Functional Analysis*, Pergamon Press, 1982.
4. Bertero, M., " Linear inverse and ill-posed problems," *Adv. Electron. Electron. Phys.*, Vol. 45, 1–120, 1989.
5. Den Dekker, A. and A. van den Bos, "Resolution: A survey" *J. Opt. Soc. Am. A*, Vol. 14, 547–557, 1997.
6. Jagerman, D., "ϵ-entropy and approximation of bandlimitated functions," *SIAM J. Appl. Math.*, Vol. 17, 362–377, 1969.
7. Toraldo di Francia, G., " Degrees of freedom of an image," *J. Opt. Soc. Am.*, Vol. 59, 799–804, 1969.
8. Piestun, R. and D. A. B. Miller, "Electromagnetic degrees of freedom of an optical system," *J. Opt. Soc. Am. A*, Vol. 17, 892–902, 2000.
9. Newsam, G. and R. Barakat, "Essential dimension as a well-defined number of degrees of freedom of finite-convolution operators appearing in optics," *J. Opt. Soc. Am. A*, Vol. 2, 2040–2045, 1985.
10. Kolmogorov, F. M. and V. M. Tikhomirov, "ϵ-entropy and ϵ-capacity of sets in functional spaces," *Am. Math. Soc. Transl.*, Vol. 17, 277–364, 1961.
11. Tikhonov, A. N. and V. I. Arsenine, *Solution to Ill-posed Problems*, Halsted, New York, 1977.
12. De Micheli, E. and G. A. Viano, "Fredholm integral equations of the first kind and topological information theory," *Integr. Equ. Oper. Theory*, Vol. 73, 553–571, 2012.
13. De Micheli, E. and G. A. Viano, "Metric and probabilistic information associated with Fredholm integral equations of the first kind," *J. Int. Eq. Appl.*, Vol. 14, 283–310, 2002.
14. Slepian, D. and H. O. Pollak, "Prolate spheroidal wave function, Fourier analysis and uncertainty I," *Bell Syst. Tech. J.*, Vol. 40, 43–63, 1961.
15. Hille, E. and J. Tamarkin, "On the characteristic values of linear integral equations," *Acta Math.*, Vol. 57, 1–76, 1931.
16. Solimene, R., M. A. Maisto, and R. Pierri, "The role of diversity on the singular values of linear scattering operators: The case of strip objects," *J. Opt. Soc. A*, Vol. 30, 2266–2272, 2013.
17. Landau, H. J., "Sampling, data transmission, and the Nyquist rate," *IEEE Proc.*, Vol. 55, 1701–1706, 1967.
18. Beurling, A. and P. Malliavin, "On the closure of characters and the zeros of entire functions," *Acta Math.*, Vol. 118, 79–93, 1967.
19. Landau, H. J., "Necessary density conditions for sampling and interpolation of certain entire functions," *Acta Math.*, Vol. 117, 35–52, 1967.
20. Solimene, R. and R. Pierri, "Localization of a planar perfect-electric-conducting interface embedded in a half-space," *J. Opt. A: Pure Appl. Opt.*, Vol. 8, 10–16, 2006.

21. Solimene, R., M. A. Maisto, and R. Pierri, "Inverse source in the presence of a reflecting plane for the strip case," *J. Opt. Soc. Am. A*, Vol. 31, 2814–2820, 2014.
22. Solimene, R., M. A. Maisto, and R. Pierri, "Inverse scattering in the presence of a reflecting plane," *J. Opt.*, Vol. 18, 025603, 2015.
23. Solimene, R., C. Mola, G. Gennarelli, and F. Soldovieri, "On the singular spectrum of radiation operators in the non-reactive zone: The case of strip sources," *J. Opt.*, Vol. 17, 025605, 2015.
24. Riesz, F. and B. S. Nagy, *Functional Analysis*, Dover Publications, 1990.